symmetry

MDPI

Article

Tuning the Cu/Ce Ratio for Improved Benzene Oxidation over Gold-Promoted Alumina-Supported CuO-CeO_2

Tatyana Tabakova [1,*], Petya Petrova [1], Yordanka Karakirova [1], Georgi Avdeev [2], Elitsa Kolentsova [3] and Lyuba Ilieva [1]

[1] Institute of Catalysis, Bulgarian Academy of Sciences, 1113 Sofia, Bulgaria
[2] Institute of Physical Chemistry, Bulgarian Academy of Sciences, 1113 Sofia, Bulgaria
[3] Department of Chemistry and Phytopharmacy, Agricultural University, 4000 Plovdiv, Bulgaria
* Correspondence: tabakova@ic.bas.bg

Abstract: Increased levels and detrimental effects of volatile organic compounds (VOCs) stimulate research efforts to develop catalysts with high efficiency in complete hydrocarbon oxidation. This work is focused on the complete oxidation of benzene as a probe reaction for VOCs elimination over alumina-supported CuO-CeO_2 mixed oxide promoted by gold. The benzene molecule is the most stable among the aromatic hydrocarbons with toxic and often carcinogenic effects known as BTEX (benzene, toluene, ethylbenzene, and xylenes) owing to the symmetry and stability of the benzene ring. Use of low-cost materials as support is an appropriate strategy aimed at improving catalyst economic profitability. The effect of the Cu-Ce ratio, namely 2:1 and 1:5, and the role of supported gold in the catalyst performance were evaluated. Analysis of the impact of support composition in benzene oxidation was based on sample characterization by textural measurements, PXRD, EPR spectroscopy, and the TPR technique. Special attention was paid to the disturbed symmetry of the ceria crystallographic structure by defects formation and its implication for the catalytic activity. Gold on alumina-supported binary oxide catalysts exhibited a significantly higher activity than promoted supported monometallic oxides. The best performance of the Au/Cu-Ce 1:5 sample was related to the highest concentration of paramagnetic Cu^{2+} ions and the best copper species dispersion evidenced by PXRD, EPR, and TPR results. The catalyst achieved stable total oxidation to CO_2 and water by 94% benzene conversion at 250 °C, thus implying the potential of this composition in developing efficient catalytic materials for atmospheric pollutant abatement.

Keywords: gold catalysts; Cu-Ce mixed oxide; complete benzene oxidation

Citation: Tabakova, T.; Petrova, P.; Karakirova, Y.; Avdeev, G.; Kolentsova, E.; Ilieva, L. Tuning the Cu/Ce Ratio for Improved Benzene Oxidation over Gold-Promoted Alumina-Supported CuO-CeO_2. *Symmetry* **2023**, *15*, 263. https://doi.org/10.3390/sym15020263

Academic Editor: Jan Cz. Dobrowolski

Received: 19 December 2022
Revised: 5 January 2023
Accepted: 13 January 2023
Published: 17 January 2023

1. Introduction

Nowadays, the increased levels and detrimental effects of volatile organic compounds (VOCs) on air quality and human health have become a serious global concern from an environmental point of view. A variety of technologies is applied to decrease harmful emissions from various chemical industries. Among them, complete oxidation to CO_2 and water at relatively low temperature is one of the most effective and environmentally friendly approaches for VOCs removal [1,2]. Rational design of catalytic materials with high effectiveness in the destructive elimination of VOCs is one of the scientific challenges. It has triggered a substantial interest in the field of environmental catalysis because efficient catalysts should combine high activity and economic profitability [3–5]. Currently, two major types of catalysts, namely noble-metal-based and transition metal oxides, are the most intensively studied to meet demanding environmental regulations [6].

Ceria and ceria-based materials are widely used in catalysis [7–9]. Very recently, Yang et al. reviewed the structure–activity relationship between defect engineering and the performance of CeO_2-based heterogeneous catalysis [10]. Structural defects, particularly oxygen vacancies, play a key role in ceria reactivity. An appropriate combination with

precious and base metals can successfully tune the unique properties of ceria. Due to the abundant availability of copper and ceria and the relatively low cost, CuO_x-CeO_2 is a very competitive catalytic material. The main effect of porosity, size, morphology, and chemical/structural modification of the CuO_x-CeO_2 binary system on the performance in many important catalytic reactions has been addressed [11,12] (and references therein). Among the variety of catalytic applications, materials consisting of copper oxide and ceria are successfully employed in deep VOCs oxidation and, generally, a higher activity compared to those of their monometallic oxide counterparts has been reported [13,14]. However, the role of copper species as highly dispersed CuO species, Cu-[O_x]-Ce structures, Cu-Ce solid solution, and isolated CuO particles as well as the ceria defect structure and interfacial interaction between Cu-Ce mixed oxides in the catalytic combustion of VOCs are still a matter of debate [15]. In addition to the important role of the preparation method, calcination procedure, Cu/Ce ratio and reaction conditions, the catalytic combustion activity is also affected by adsorption and activation of the pollutant molecule depending on its chemical nature [4]. Aromatic hydrocarbons represent toxic and often carcinogenic VOCs. Benzene, toluene, ethylbenzene, and xylenes (BTEX) contribute to the majority of total industrial emissions. Supported Cu-Ce binary oxides [16–18] and CuO-CeO_2 composites prepared by different methods [19–24] were most extensively studied in the complete oxidation of toluene. Because of the lower reactivity, benzene seems even more appropriate as a representative molecule for BTEX combustion. The benzene molecule is the most stable as the addition of ethyl or methyl groups affects the π-electron structure, disrupting the symmetry and stability of the benzene ring. Zhou et al. established the lowest catalytic conversion of benzene as compared to other studied BTEX over a Ce-Cu oxide catalyst with an optimal Ce/Cu ratio of 1:1 prepared by a hard-template method [25]. According to an earlier study of benzene, toluene, and xylene oxidation [26], a 5 wt.% Cu/γ-Al_2O_3 sample showed the best performance among various alumina-supported metal oxides with activities as follows: toluene > xylene > benzene. Therefore, an efficient catalyst for benzene combustion can guarantee successful abatement of other BTEX pollutants.

Hu et al. [27] showed that the mesoporous CuO-CeO_2 catalyst with large surface area prepared by a template method exhibited complete benzene oxidation to CO_2 and water at 250 °C. However, water vapor affected the mesoporous structure in a detrimental way and the catalytic activity sharply decreased during the time on stream. Later, the same group synthesized CuO-CeO_2 binary oxides with a plate-like morphology using the solvothermal method. A high and stable catalytic activity during complete benzene oxidation at 240 °C was reached despite the relatively low surface area. The presence of large amounts of CuO species on the surface of CuO-CeO_2 nanoplates with stable structure was suggested to affect catalytic performance [28]. Jung et al. [29] studied benzene deep oxidation over nanocrystalline powders of CuO-CeO_2 oxides synthesized via the combustion method with organic fuel, and 100% conversion was observed at about 350 °C over the catalyst with an optimal Cu/(Cu + Ce) ratio of 3. Very recently, Hou et al. [15] characterized systematically a series of Cu-Ce mixed oxides of variable molar ratio prepared by the sol–gel method. The best catalytic performance in benzene combustion was achieved over a catalyst with Cu/Ce = 1 (T_{90} = 260 °C).

Rational design of highly efficient catalysts is closely related to the use of low-cost materials as support. An effective approach to tuning the catalytic performance by control of the exposed active sites is deposition of transition metal oxide or mixed oxides on the support surface. Recently, we demonstrated that promotion of alumina-supported Cu-Mn mixed oxide by gold was an advantageous strategy for the preparation of catalysts with high efficiency in pollutant removal from waste gases of formaldehyde production [30]. Gold, regarded as inappropriate from a catalytic point of view because of its chemical inertness, became a subject of appreciable research for the last three decades. It attracted significant interest due to the surprisingly high activity of supported gold particles (less than 10 nm) in a variety of processes including VOCs oxidation [31–39].

The aim of the present work was to study complete benzene oxidation (CBO) over Al_2O_3-supported CuO-CeO_2 mixed oxide promoted by gold. The investigation focused on the effect of various Cu/Ce molar ratios on benzene conversion. The selection of these ratios was based on our previous studies. The impact of Cu-Mn sample composition on CO oxidation activity was systematically investigated and the best performance was demonstrated by samples with Cu/Mn ratios of 2:1 and 1:5 [40]. Later, the effect of cerium modification on the activity and selectivity of alumina-supported CuO-MnO_2 catalysts with Cu/Mn molar ratios of 2:1 and 1:5 for total oxidation of CO was studied [41]. In this work, Mn was replaced by Ce in the whole concentration range from 0 to 100%. Although the Cu-Mn catalytic system is considered very active in CO oxidation, samples with totally replaced Mn exhibited the best activity, i.e., Cu-Ce with molar ratios of 2:1 and 1:5. To the best of our knowledge, gold promotion of CuO-CeO_2 mixed oxide on alumina has not been studied in the benzene oxidation reaction. The relationship between performance for CBO and catalyst physical and chemical features determined by the mixed oxides composition is discussed.

2. Materials and Methods

2.1. Catalyst Preparation

Wet impregnation of γ-Al_2O_3 (fraction 0.6−1.0 mm calcined for 2 h at 450 °C) with a solution of $Cu(NO_3)_2.3H_2O$ (Merck, Rahway, NJ, USA) and $Ce(NO_3)_3.6H_2O$ (Sigma-Aldrich, Burlington, VT, USA), properly mixed to guarantee Cu:Ce molar ratios of 2:1 and 1:5 in the composition (20 wt.% active phase in total), was performed at 80 °C within 12 h. Thermal treatment included drying at 120 °C for 10 h and calcination at 450 °C for 4 h. Additionally, CuO/Al_2O_3 and CeO_2/Al_2O_3 (20 wt.%) were prepared following the same procedure for comparative purposes. Depending on composition, the samples were denoted as Cu-Ce 2:1, Cu-Ce 1:5, CuO/Al_2O_3, and CeO_2/Al_2O_3.

The deposition-precipitation method was used for preparation of gold-containing samples on well-water-suspended carriers by using ultrasound. Gold (2 wt.%) deposition was performed through simultaneous addition of an aqueous solution of $HAuCl_4 \cdot 3H_2O$ (Sigma-Aldrich) and Na_2CO_3 (Merck) into the reactor at a constant temperature of 60 °C and a pH of 7.0 under stirring. Suspensions were agitated at 60 °C for 1 h and then filtered and washed to remove remaining chlorine ions. The samples thus obtained were dried in vacuum at 80 °C and calcined at 400 °C for 2 h. Gold on alumina was also synthesized for comparison. Depending on the composition of the solids used as support, the samples were denoted as Au/Cu-Ce 2:1, Au/Cu-Ce 1:5, Au/CuO/Al_2O_3, Au/CeO_2/Al_2O_3, and Au/Al_2O_3.

2.2. Catalyst Characterization

Textural characteristics of the catalysts were estimated by low-temperature (−196 °C) nitrogen adsorption/desorption experiments carried out by using a NOVA 1200e Quantachrome Instruments analyzer (Boynton Beach, FL, USA). Prior to the measurements, the samples were degassed under vacuum at 200 °C for 2 h. The specific surface area (SSA) calculation was based on analysis of the N_2 adsorption isotherm using the Brunauer, Emmett, and Teller (BET) equation. The Barrett, Joyner, and Halenda (BJH) method was used to estimate total pore volume (V_{pore}) and average pore diameter (d_{pore}).

Powder X-ray diffraction (PXRD) patterns were recorded on PANalytical Empyrean apparatus equipped with a multichannel detector (Pixel 3D, PANalytical B.V., Almelo, The Netherlands) using Cu K_α radiation in the range 20–90° 2θ with a scan step of 0.01° for 20 s. Particle sizes of the crystalline phases and cell parameters were evaluated by powder diffraction analysis software based on the Rietveld method (ReX) [42]. All refinements ended up with satisfactory statistical criteria. Rp (residual of least-squares refinement) ranged from 5 to 6 and GOF (goodness of fit) was around 2.

Electron paramagnetic resonance (EPR) spectra were collected on a JEOL JES-FA 100 (JEOL, Tokyo, Japan) EPR spectrometer operating in the X–band frequency ($\nu \approx 9.4$ GHz)

with 100 kHz field modulation. The instrument was equipped with a standard TE_{011} cylindrical resonator. The sample (40 mg) was taken in a special quartz EPR tube with i.d. = 3 mm. The spectra were recorded at room temperature and low temperature (123 K). Changes in spectral resolution were not observed at lower temperatures.

Temperature-programmed reduction (TPR) measurements were performed in a flow system equipped with a thermal conductivity detector using an H_2-Ar mixture (10% H_2) at a flow rate of 24 mL min^{-1} and temperature ramp rate of 15 °C min^{-1} as described in Ref. [38]. The loaded sample amount was 0.05 g.

2.3. Catalytic Activity Measurements

The catalytic activity was expressed as benzene conversion degree. Prior to the catalytic measurements, catalyst activation was conducted in situ at 200 °C for 1 h by purified air following the findings of Yu et al. for the contribution of such a procedure to the abundance of loosely bonded molecular oxygen species [43]. Conversion degree was measured at atmospheric pressure over the temperature range of 150–300 °C in a microcatalytic continuous-flow fixed-bed reactor connected to a gas chromatograph Hewlett Packard 5890 series II (Agilent, Germany, working with Agilent G2070 Chemstation Software, Waldbronn, Germany) supplied with a flame ionization detector and capillary column HP Plot Q. The measurements were carried out using a catalyst with a bed volume of 0.5 cm^3 and particle size of 0.25–0.50 mm, inlet benzene concentration of 42 g m^{-3} in air, and space velocity of 4000 h^{-1}. A long-term stability test over gold-containing catalysts at 300 °C was carried out within 24 h.

Benzene conversion degree was calculated by the equation:

$$C_6H_6 \text{ conversion } (\%) = \frac{[C_6H_6]_{in} - [C_6H_6]_{out}}{[C_6H_6]_{in}} \times 100, \quad (1)$$

where $[C_6H_6]_{in}$ and $[C_6H_6]_{out}$ are the benzene concentrations at the reactor inlet and outlet, respectively.

3. Results

3.1. Sample Characterization

Textural parameters of the studied samples are listed in Table 1. Impregnation of γ-alumina with aqueous solutions of mono- or bi-component Cu-Ce nitrates led to lower values of specific surface area (SSA), total pore volume (V_{pore}), and average pore diameter (D_{pore}) as compared to those of the primary carrier. The observed changes could be explained through alumina pore blocking due to the formation of single oxide or binary oxide phases into the pores. A slight increase in SSA was registered after deposition of gold. This effect was better pronounced in the case of $Au/CuO/Al_2O_3$ and Au/Cu-Ce 1:5, with SSA about 10 m^2 g^{-1} higher relative to the matching support. The presence of well-defined mesopores with a narrow pore size distribution was shown through analysis of the adsorption–desorption isotherm and the corresponding pore size distribution parameter. These textural characteristics were almost the same after promotion by gold.

PXRD patterns of samples with a molar ratio of Cu-Ce 2:1 with and without gold are presented in Figure 1a. X-ray diffractograms of CuO/Al_2O_3, $Au/CuO/Al_2O_3$, and CeO_2/Al_2O_3 are also displayed for comparison. Well-visible reflections in the XRD patterns of CuO/Al_2O_3 and $Au/CuO/Al_2O_3$ were positioned at 2θ = 35.6, 38.8, 48.6, and 61.8° (marked with *) and related to CuO. The shape of the peaks evidenced a high degree of crystallinity of the CuO particles. The peaks position of CeO_2/Al_2O_3 at 2θ = 28.5, 33.2, 47.7, and 56.6° (marked with o) were, respectively, assigned to (111), (200), (311), and (222) planes of the face-centered cubic fluorite structure of ceria. CuO and CeO_2 XRD diffraction intensities decreased significantly in the pattern of the Cu-Ce 2:1 sample, indicating improved dispersion of both separate phases. This phenomenon could be attributed to the formation of smaller CuO crystallites in agreement with the well-known property of ceria to favor the high dispersion of supported metal particles. Indeed, calculation of the average

crystallite size of CuO (D_{CuO}) (Table 1) revealed the formation of particles of smaller size. A value of 33.4 nm was estimated from X-ray line broadening of the peaks at 2θ = 35.6 and 38.8° in CuO/Al_2O_3, while D_{CuO} was 23.0 nm in the Cu-Ce 2:1 sample.

Table 1. Specific surface area (SSA), pore volume (V_{pore}), average pore diameter (D_{pore}), average particles size of CeO_2 (D_{CeO2}) and CuO (D_{CuO}), and lattice parameter of CeO_2 (a_{CeO2}) estimated by XRD.

Sample	SSA ($m^2\ g^{-1}$)	V_{pore} ($cm^3\ g^{-1}$)	D_{pore} (nm)	D_{CeO2} (nm)	D_{CuO} (nm)	a_{CeO2} (Å)
Al_2O_3	219	0.40	7.0	-	-	-
CuO/Al_2O_3	173	0.43	9.5	-	33.4	-
CeO_2/Al_2O_3	159	0.36	9.4	8.8 (3) [1]	-	5.407 (3)
Cu-Ce 2:1	156	0.29	7.3	5.4 (3)	23.0	5.434 (5)
Cu-Ce 1:5	165	0.29	7.0	7.6 (4)	n.d.	5.413 (1)
$Au/CuO/Al_2O_3$	182	0.40	9.2	-	26.2	-
$Au/CeO_2/Al_2O_3$	161	0.36	9.4	9.0 (1)	-	5.410 (2)
Au/Cu-Ce 2:1	159	0.28	7.1	5.4 (5)	n.d.	5.443 (3)
Au/Cu-Ce 1:5	176	0.28	6.5	6.3 (2)	n.d.	5.420 (1)

[1] Figures in parentheses give the error of the last listed decimal digit. n.d.—not detected.

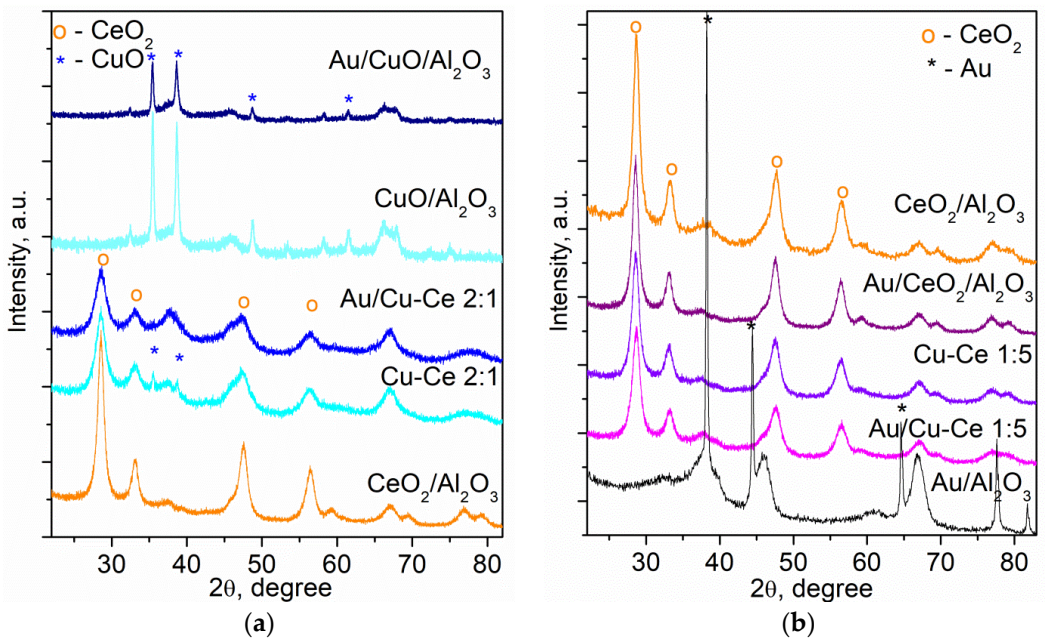

Figure 1. PXRD patterns of the studied samples: (**a**) with a molar ratio of Cu-Ce 2:1 with and without gold, CuO/Al_2O_3, $Au/CuO/Al_2O_3$, and CeO_2/Al_2O_3; (**b**) with a molar ratio of Cu-Ce 1:5 with and without gold, CeO_2/Al_2O_3, $Au/CeO_2/Al_2O_3$, and Au/Al_2O_3.

Figure 1b displays PXRD patterns of samples with a molar ratio of Cu-Ce 1:5 and Au/Cu-Ce 1:5. X-ray diffractograms of CeO_2/Al_2O_3, $Au/CeO_2/Al_2O_3$, and Au/Al_2O_3 are also shown. Ceria diffraction peaks dominated in the XRD patterns of all CeO_2-containing samples. The average crystallite size of CeO_2 (D_{CeO2}) in CeO_2/Al_2O_3 and $Au/CeO_2/Al_2O_3$ was 8.8 and 9.0 nm, respectively. A tendency of lower CeO_2 crystallite size was observed for all samples based on Cu-Ce mixed oxide. Diffraction lines of crystalline CuO phase were not observed in the pattern of the Cu-Ce 1:5 sample, implying a high dispersion of copper oxide particles. Other possible reasons could be amorphization or Ce-Cu solid solution formation.

Reflections indicating the presence of crystalline gold were registered only in the pattern of Au/Al_2O_3 (Figure 1b). Strong diffraction peaks at 2θ = 38.2, 44.4, 64.6, and 77.5° were registered due to the formation of quite large gold particles with an average size of

about 32 nm. Concerning gold size in CuO-containing samples, it should be taken into account that the intense CuO (111) reflection lies at the same angle as the most intense peak of Au (111) located at 2θ = 38.2°. In this case, the CuO reflection would preclude gold identification even if any peak existed. A comparison of experimental and theoretical XRD patterns of Au/Cu-Ce 2:1 and Au/Cu-Ce 1:5 is reported in Supplementary material (Figures S1, a and b, respectively) as an experimental proof of gold deposition. The lack of diffraction at 2θ = 44.4 and 64.6° allows one to assume the formation of highly dispersed gold particles in all samples. The result gives evidence again for ceria's effect on noble metal dispersion. It also confirms the observation of Wolski et al. [44] that copper species could preserve gold particle aggregation during calcination.

Considering the important role of gold particle size on the catalytic activity, many studies involve TEM measurements. However, the TEM determination of gold particle size on CeO_2-containing supports is complicated as ceria dark contrast prevents the nanoparticles from being accurately detected [45] and a combination with HAADF should be used. In the present case of highly dispersed gold particles, the exactly measured differences in average particle size, particularly size distribution histograms, are not decisive to explain the catalytic behavior of gold-promoted alumina-supported CuO-CeO_2.

Comparison between ionic radii of Ce^{4+} (0.97 Å) and Cu^{2+} (0.73 Å) suggests the possibility of forming a Ce-Cu solid solution. Replacement of Ce^{4+} by low-valent copper ions implies a spontaneous formation of oxygen vacancies for charge balance, distortion of ceria structure through transformation of adjacent Ce^{4+} into Ce^{3+}, resulting in the generation of another oxygen vacancy, and increased microstrains [46,47]. Some researchers have reported shrinkage of the ceria lattice resulting from the replacement of Ce^{4+} ions by Cu^{2+} ions with smaller ionic radius. A small shift in ceria XRD peak at 2θ = 28.5° to higher Bragg angles was considered experimental evidence of copper species incorporation into the ceria lattice [15,21,47]. A tendency of lattice contraction was observed in the magnified patterns in the 2θ range of 26−32° of both Cu-Ce mixed oxide compositions and gold-containing samples (Figure 2a,b), thus focusing on Cu^{2+} substitution for Ce^{4+} and the formation of defects in the ceria lattice. The solubility of Cu ions in CeO_2 is limited [48]. Excessive copper formed a CuO phase registered in the case of the Cu-Ce 2:1 catalyst with a higher copper content.

Analysis of PXRD data reported in Table 1 revealed a slight increase in the CeO_2 unit cell parameter (a_{CeO2}) of both mixed oxide compositions and corresponding gold-containing samples as compared to 5.407 Å of bare ceria on alumina. Our results are consistent with Shim et al. who observed ceria lattice expansion in CeO_2-promoted Cu/Al_2O_3 attributed to an increased amount of Ce^{3+} with an ionic radius of 1.10 Å in comparison with 0.97 Å of Ce^{4+} [49]. A close correlation between Ce^{3+} content and oxygen vacancies concentration was discussed by Konsolakis and Lykaki [12] (p. 7). The authors pointed out an inverse relationship between ceria particle size and cell parameter resulting from increased Ce^{3+} content and oxygen vacancy concentration. In good agreement with this finding, our calculations showed the lowest particle size of ceria (5.4 nm) and the highest lattice parameter, namely 5.434(5) and 5.443(3) Å for Cu-Ce 2:1 and Au/Cu-Ce 2:1, respectively. However, it should be noted that ceria cell expansion is opposite to the contraction resulting from Cu^{2+} insertion into the ceria cell. The combination of both effects has been commented on by Tsoncheva et al. to explain the preservation of the ceria unit cell parameters of Cu-Ce bi-component materials [18]. In our case, we could hypothesize that ceria's particle-size effect plays a more decisive role upon structural defect formation, which affects beneficially benzene oxidation activity.

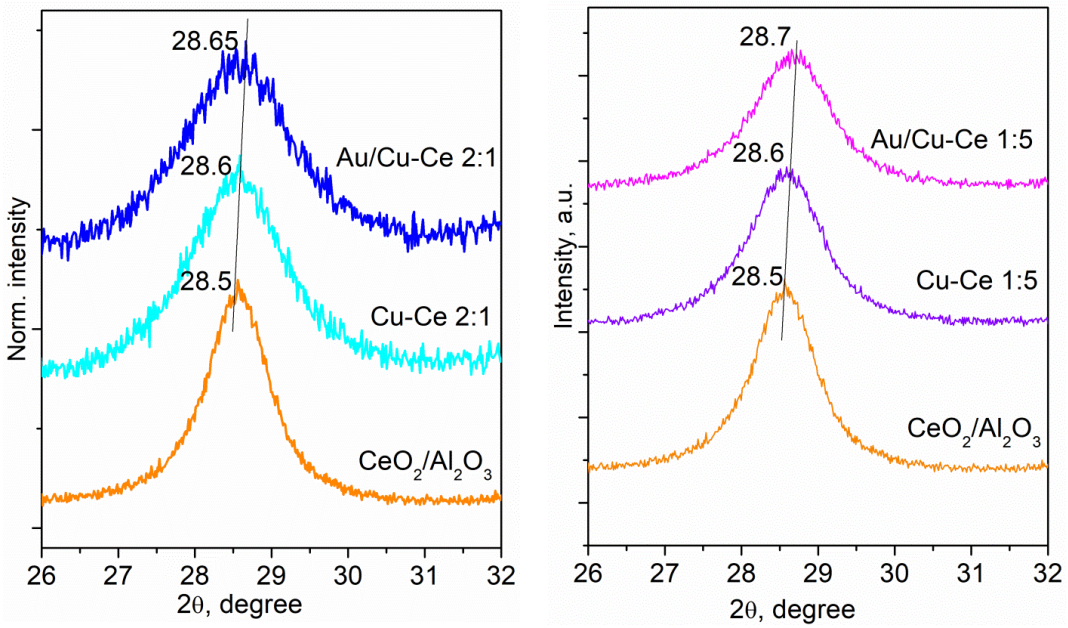

Figure 2. PXRD magnified pattern of CeO_2 (111) in 2θ range of 26–32°: (**a**) samples with a molar ratio of Cu-Ce 2:1 with and without gold; (**b**) samples with a molar ratio of Cu-Ce 1:5 with and without gold.

The literature data show that X-ray photoelectron (XP) spectroscopy is often used to investigate the copper oxidation state. However, based on our experience with characterization of CuO/ceria catalysts [50], the analysis of Cu 2p XP spectra of samples with low Cu/Ce ratios such as the present case of a Cu/Ce ratio of 1:5 is complicated because the shake-up satellite signals characteristic for the Cu^{2+} oxidation state became undetectable. Keeping this in mind, all copper-containing samples were analyzed by EPR spectroscopy, which is a very sensitive and reliable technique to analyze the oxidation state of copper. EPR spectra collected at room temperature have an identical shape typical of Cu^{2+} ions (Figure 3). Spectral parameters, namely g factors, line widths (H), and peak-to-peak signal amplitudes (I) are presented in Table 2. Signals with these parameters correspond to isolated, monomeric Cu^{2+} species on the catalyst surface characterized by axial spectra with resolved hyperfine features in the parallel region [51]. Hyperfine features in the perpendicular region are not observed. As can be seen in Table 2, spectral parameter values are similar. An exception is the line width of Cu-Ce 1:5 and Au/Cu-Ce 1:5 samples where the EPR signal is narrower than those of the other samples. This result could be attributed to better dispersion of the Cu^{2+} ions in Ce-rich composition. Recently, a low intense line at a g value of 1.9677 was observed in the EPR spectrum of the CuO/CeO_2 (3 wt.% Cu) sample [50]. The line was assigned to Ce^{3+} ions formed during the water–gas shift reaction. However, no signal due to cerium ions was registered in the present study, possibly due to a very intense CuO signal.

Gold deposition preserved the shape of the EPR spectra but affected the peak-to-peak signal amplitude, i.e., their intensity. This parameter provides reliable information about the relative concentration of paramagnetic Cu ions in the samples. The highest values were measured with the spectra of Cu-Ce 1:5 and Au/Cu-Ce 1:5, evidencing an abundance of active Cu^{2+} centers (Table 2). The EPR signal intensity decreased slightly in the spectrum of Au/Cu-Ce 2:1 relative to Cu-Ce 2:1. This finding could be ascribed to the formation of diamagnetic copper ions (Cu^{+}) or copper clusters of diamagnetic nature.

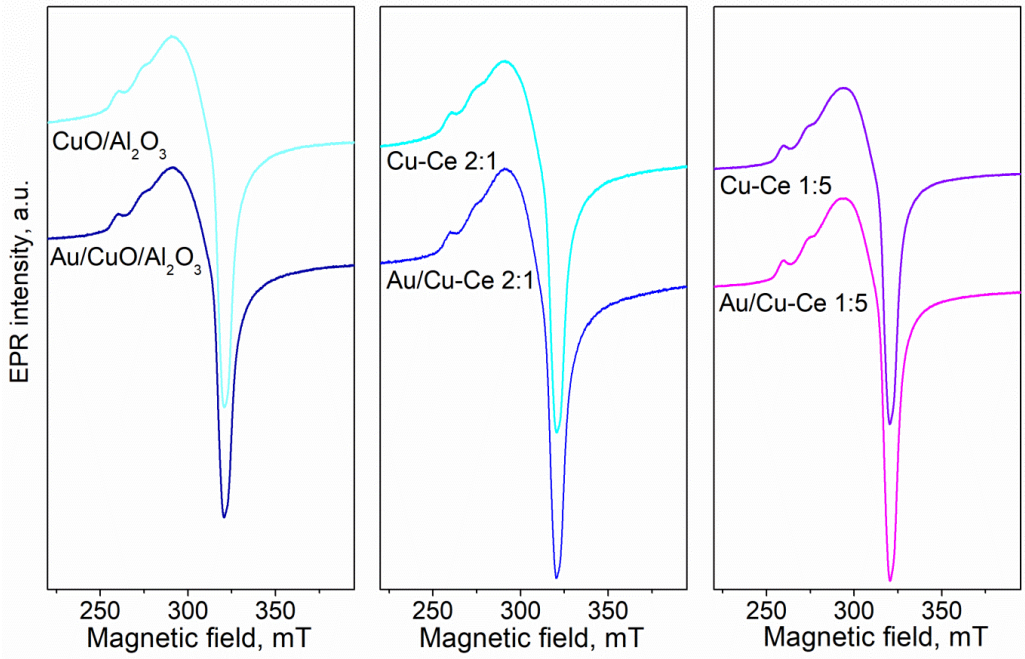

Figure 3. EPR spectra of the studied samples.

Table 2. Parameters of the EPR spectra shown in Figure 3.

Sample	g_{II}	$g_{\perp}$	ΔH (mT)	I (a.u.)
CuO/Al_2O_3	2.3317	2.0759	29.85	1140
Cu-Ce 2:1	2.3361	2.0753	29.53	1138
Cu-Ce 1:5	2.3329	2.0751	26.18	1990
$Au/CuO/Al_2O_3$	2.3316	2.0762	29.69	1075
Au/Cu-Ce 2:1	2.3377	2.0751	29.38	1037
Au/Cu-Ce 1:5	2.3342	2.0741	26.29	2482

H_2-TPR analyses were performed to compare the sample reducibility depending on catalyst composition. TPR profiles of alumina-supported CuO, CeO_2, and binary oxides Cu-Ce 2:1 and Cu-Ce 1:5 are illustrated in Figure 4a. It is well known that surface layer reduction of bare ceria proceeds at around 500 °C, while bulk reduction occurs at about 800 °C [52]. The proposed limit of surface reduction without changing the fluorite structure is 20% [53]. A low intense TPR peak below 400 °C in the profile of CeO_2/Al_2O_3 indicated enhanced surface reduction. It could be related to the presence of small ceria crystallites formed on alumina [16]. According to the literature, a single TPR peak with T_{max} in the range of 260–300 °C is attributed to bulk reduction of CuO of different particle sizes [54–56]. A one-step reduction to Cu^0 is also accepted for CuO loaded on alumina. The presence of more reduction peaks instead of one for pure CuO is related to structural differences in a variety of supported copper oxide species [26]. Two TPR peaks in the profile of CuO/Al_2O_3 with T_{max} at 206 °C and 247 °C (Figure 4a) could be reasonably explained by the presence of CuO with different dispersions [16] (and references therein). In general, the reduction process of $CuO\text{-}CeO_2$ binary oxides is facilitated as compared to individual CeO_2 and CuO counterparts [11]. It is accepted that CeO_2 promotes the reduction of CuO phase in close vicinity [19,29] (and references therein). On the other hand, transition metals such as copper promote the surface reduction of CeO_2 [57]. Improved reducibility was explained by hydrogen activation over already formed metallic copper and hydrogen spillover from Cu sites to ceria [58].

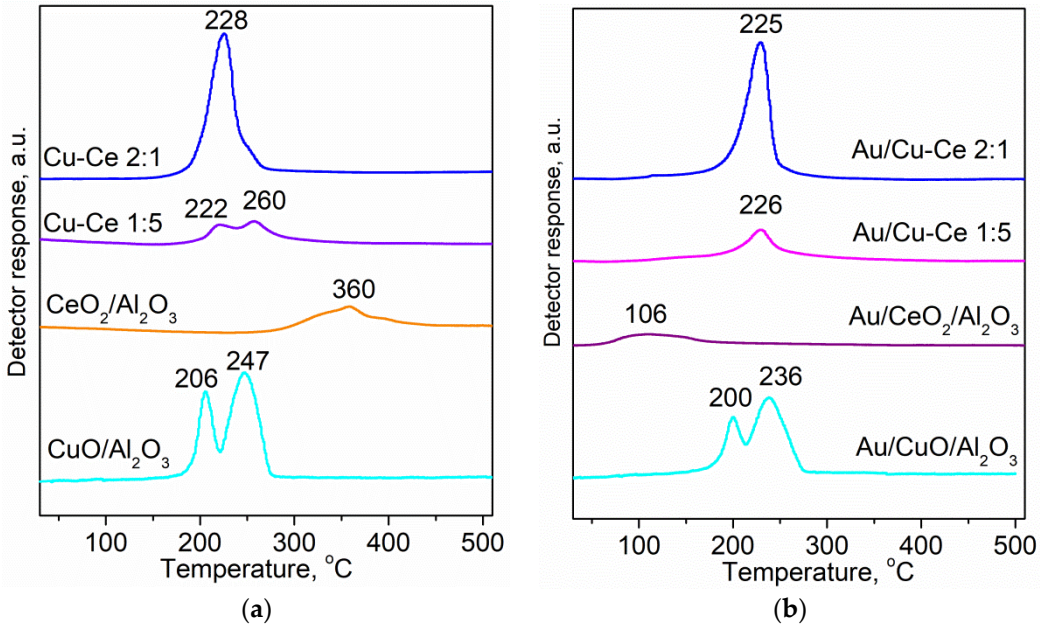

Figure 4. TPR profiles of: (**a**) alumina-supported mono and binary oxides; (**b**) gold-promoted samples.

Few authors have assigned reduction peaks of CuO-CeO_2 catalysts to a two-step CuO reduction process [59] (and references therein). However, it was more commonly accepted that the registration of various TPR peaks depended on proven different types of Cu-containing species. In general, small-sized CuO particles are easily reducible in contrast with higher aggregation forms [60]. The TPR peak at the lowest temperature was commonly ascribed to highly dispersed CuO_x species [15,20,27,28,47]. CuO clusters and Cu ions strongly interacting with the ceria surface were also considered [19,55]. Undoubtedly, the TPR peak at the highest temperature was related to the reduction of bulk-like CuO particles weakly associated with CeO_2 [19,20,23,29,47,55]. Some authors also reported the appearance of a third reduction peak at moderate temperature ascribed to Cu ions incorporated into the ceria cell [23,57,61]. By contrast, Sun et al. [56] registered four TPR peaks and the last one was associated with Cu^{2+} reduction in the ceria lattice. Many authors commented only on the TPR peak assignment related to the copper oxide phase. However, the overlapping with hydrogen consumption due to enhanced ceria surface reduction in the same range should also be considered.

The main TPR peak at T_{max} = 228 °C in the profile of Cu-Ce 2:1 (Figure 4a) can be assigned to the CuO → Cu^0 reduction of larger crystallites detected by XRD. The profile also comprised a lower temperature reduction of highly dispersed copper species. A shoulder at around 250–260 °C should be related to ceria surface layer reduction. It proceeded at a lower temperature as compared to that in CeO_2/Al_2O_3 due to the promotional effect of metallic copper being formed during the reduction. The profile of the Cu-Ce 1:5 sample was governed by the variation in sample composition, particularly the lack of XRD-detectable CuO phase. The first weak peak with T_{max} at 222 °C corresponded to the reduction of highly dispersed CuO species and isolated Cu^{2+} ions. This conclusion is based on EPR evidence for available highly dispersed copper ions. The contribution of copper reduction to Cu-O-Ce structures could also be considered. The TPR peak with T_{max} at 260 °C should be related to hydrogen consumption due to the reduction of oxygen from ceria surface layers.

Deposition of small gold particles undetectable by PXRD improved the reducibility of the alumina-supported oxides (Figure 4b), which was in favor of benzene oxidation. Gold affected most significantly the mobility of ceria surface oxygen as demonstrated by a TPR peak at 106 °C in line with the well-known role of nano-gold in boosting the ceria surface layer reduction [62]. Such a shift to lower temperature could also be assumed in the case of Au/Cu-Ce 2:1 and Au/Cu-Ce 1:5 because the shoulder of the main peak in the profile of Cu-Ce 2:1 and the weak peak located at about 250 °C in the profile of Cu-Ce 1:5

disappeared. However, expected lower-temperature TPR peaks in the profiles of Au/Cu-Ce 2:1 and Au/Cu-Ce 1:5 were not registered. It was reasonable to suggest that hydrogen consumption for surface reduction of very low ceria amounts was beyond measurement sensitivity. Furthermore, gold deposition caused a lowering of peak intensity. This effect was clearly visible on comparing CuO/Al_2O_3 and $Au/CuO/Al_2O_3$ profiles. A possible explanation could be Au-Cu alloy formation resulting from the interaction between gold and copper metallic particles in the presence of hydrogen. Our previous TPR studies of Au-Pd catalysts for CBO showed the formation of inactive intermetallic species having a lesser effect on reducibility [63]. Based on a shift in the XRD peak typical of monometallic gold toward high angles, an Au-Cu alloy-like structure in the studied bimetallic samples was evidenced after hydrogen treatment above 200 °C [64,65]. However, the interaction between metallic copper and gold could not occur during the reaction of benzene oxidation in excess of oxygen.

3.2. Catalytic Activity in Benzene Oxidation

The benzene oxidation activity of alumina-supported single (CuO and CeO_2) and Cu-Ce mixed oxides and matching gold-promoted samples as C_6H_6 conversion degree depending on temperature is illustrated in Figure 5. Any products of incomplete oxidation were not registered in all cases. Comparison of 'light off' curves of the catalysts presented in Figure 5a evidenced a strong effect of composition on catalyst activity. CeO_2/Al_2O_3 exhibited better performance than CuO/Al_2O_3 at temperatures below 250 °C. The same result was reported by Hou et al. [15] and explained by the crucial role of temperature for the catalytic activity of CuO [66]. A significantly higher activity compared to that of single-component counterparts was observed in the whole temperature interval with Cu-Ce 1:5, while Cu-Ce 2:1 exhibited such behavior above 250 °C. A cerium-rich sample showed enhanced performance as compared to the copper-rich one yielding 55% C_6H_6 conversion at 220 °C vs. 18% with Cu-Ce 2:1 and 77% at 250 °C vs. 28% with Cu-Ce 2:1. Finally, the samples attained 84% and 76% benzene conversion at 300 °C.

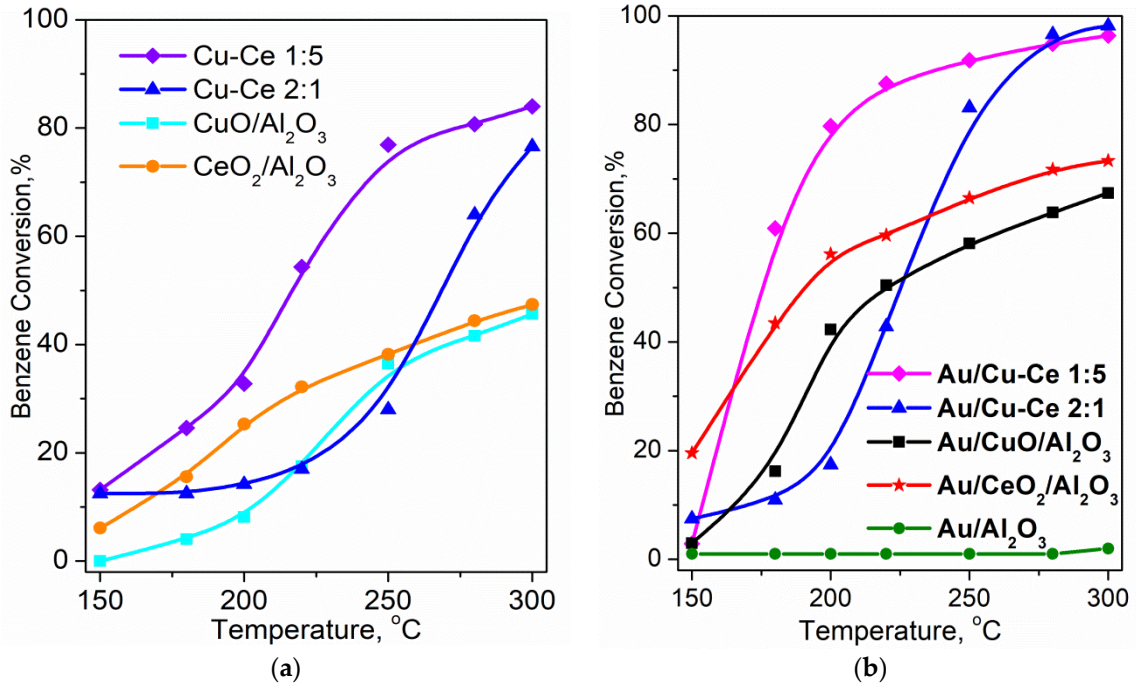

Figure 5. Temperature dependence of benzene conversion over: (**a**) alumina-supported mono- and bi-component Cu-Ce oxides; (**b**) gold-containing catalysts.

Gold on alumina-supported binary oxide catalysts exhibited a substantially higher activity than those on supported single-metal oxides. A significant effect of gold on

accelerating the benzene conversion was observed. An enhanced activity was registered at increased reaction temperature upon reaching 90% benzene conversion at 220 and 260 °C over Au/Cu-Ce/Al_2O_3 with Cu-Ce ratios of 1:5 and 2:1, respectively. The observed activity of Au/Cu-Ce 2:1 was slightly higher than that of Au/Cu-Ce 1:5 at 300 °C in agreement with the above-mentioned increased CuO activity at elevated temperatures. Table S1 reports the benzene conversion degree depending on the temperature over the studied samples. Table S2 summarizes the catalytic performance of our samples and those in the reported literature.

Additionally, these catalysts demonstrated good stability by maintaining the same degree of benzene conversion during a 24 h test at 300 °C (Figure S2). The catalytic performance of Au/Al_2O_3 demonstrated clearly the importance of gold particle size and the nature of the support. The formation of quite large metallic gold particles and non-reducible alumina support are responsible for the very poor catalytic activity of Au/Al_2O_3.

4. Discussion

The literature data revealed a different role of copper species in VOCs total oxidation over CuO-CeO_2 catalysts. A consensus of opinion is that larger CuO particles do not enhance the catalytic activity, while the high performance is related to the presence of well-dispersed surface CuO_x species [16–18,23,26,29].

Two favored geometries were accepted for the copper-ceria interaction. They were attributed to the already commented formation of Ce-Cu solid solution and the interaction between CuO and lattice vacant sites (O_{vac}) [46]. Our previous Raman spectroscopy results confirmed the role of oxygen vacancies on the ceria surface as sites for CuO-ceria interaction [50]. These structures were denoted as Cu-[O_x]-Ce and considered a bridge for oxygen transfer due to the cycle of oxygen vacancy generation and replenishment [15] (and reference therein). How and co-workers [15] proposed a pathway for benzene oxidation based on the detailed characterization of CuO-CeO_2 catalysts of different composition. The authors indicated that highly dispersed CuO_x species were the main active sites for oxidation to intermediates, CO_2 and H_2O, while Cu-[O_x]-Ce structures provided an effective oxygen supply. The Cu-[O_{vac}]-Ce species formed was recovered by gas phase oxygen.

Apart from the dependence on the active oxygen provision, the oxidation activity was also related to adsorption and activation of the reactant molecule. Experimental evidence presented that the adsorption sites for benzene molecules were not copper-containing species but defects as oxygen vacancies related to Ce^{3+} on ceria surface.

The catalytic results in the present work are in accordance with aforementioned observations. Incorporation of Cu ions into the lattice of CeO_2 was proven by a small shift in the ceria main XRD peak to higher Bragg angles in the patterns of all Cu-Ce containing samples (Figure 2a,b), revealing defect formation, particularly Ce^{3+} ions and oxygen vacancies. This phenomenon determines the tendency of ceria cell expansion (Table 1) and agrees with the particle size dependence. As already commented on in the analysis of PXRD data, an increase in Ce^{3+} content and oxygen vacancy concentration occurred with a decrease in nanoceria size due to the higher population of oxygen vacancies in particles of smaller size [67]. The correlation is more noticeable for Cu-Ce 2:1 and Au/Cu-Ce 2:1 catalysts. The created defects favor benzene adsorption and active oxygen supply. However, the availability of copper species among which highly dispersed CuO_x serve as the main active sites plays a crucial role in benzene oxidation activity. In the case of Cu-Ce 2:1 composition, the worst CBO performance could be explained by low CuO_x dispersion owing to an inactive bulk CuO phase detected by PXRD. In addition, TPR intensity profiles confirmed also the presence of larger crystallites. Copper agglomeration was not observed for the ceria-rich composition Cu-Ce 1:5. EPR results revealed better dispersion of Cu^{2+} ions and the highest concentration of paramagnetic Cu^{2+} centers in Cu-Ce 1:5 and Au/Cu-Ce 1:5 catalysts, thus correlating well with the complete benzene oxidation activity order.

The beneficial role of gold is clearly visible by comparing the corresponding 'light off' curves (Figure 5a,b). The remarkable activity indicates a promotional effect resulting from

the combination between transition metal oxides and gold nanoparticles, which contributes to the creation of new adsorption sites at Au-MO_x interfaces. It is also in line with the well-known ability of nanogold to enhance significantly the mobility of oxygen in ceria surface layers, thus accelerating the process of oxygen vacancy formation and replenishment in Cu-[O_x]-Ce structures, as well as at the vacant locations at the ceria surface participating as active sites for benzene adsorption.

The results pointed out a promising performance of these catalytic systems for abatement of environmental pollutants. Future research efforts will be directed to optimization of the catalyst composition aiming at improving economic profitability and lowering the operating costs by decreasing the temperature for complete benzene oxidation without harmful side products.

5. Conclusions

Complete oxidation of benzene as a probe reaction for VOCs elimination over alumina-supported CuO-CeO_2 mixed oxide promoted by gold was studied. The effect of various Cu/Ce ratios, namely 2:1 and 1:5, and the role of supported gold nanoparticles were investigated. Catalytic activity was greatly influenced by sample composition. Catalytic tests demonstrated that the Cu-Ce 1:5 configuration outperformed the catalytic behavior of the single-component counterparts in the whole temperature interval, while Cu-Ce 2:1 exhibited such a behavior above 250 °C. Incorporation of Cu ions into the ceria lattice was proven by a small shift in the ceria main XRD peak in the patterns of all Cu-Ce-containing samples, evidencing defect formation, particularly Ce^{3+} ions and oxygen vacancies. Promotion by gold provided additional benefits to the benzene conversion. Gold on alumina-supported binary oxide catalysts exhibited a substantially higher activity than promoted supported monometallic oxides. Our findings revealed a crucial role of highly dispersed CuO_x for benzene oxidation activity. The highest concentration of paramagnetic Cu^{2+} ions and the best dispersion of CuO in Cu-Ce 1:5 and Au/Cu-Ce 1:5 correlate well with the best performance among alumina-supported oxides and gold-containing catalysts, respectively. Gold nanoparticle availability contributed to enhanced mobility of oxygen in ceria surface layers, thus facilitating the process of oxygen vacancy formation and replenishment.

Supplementary Materials: The following supporting information can be downloaded at: https://www.mdpi.com/article/10.3390/sym15020263/s1, Figure S1. Experimental (red) and theoretical (black) XRD pattern, and peak fitting of the sample: (a) Au/Cu-Ce 2:1 and (b) Au/Cu-Ce 1:5. Difference plot is also shown (magenta). Figure S2. Comparison of catalyst stability in complete benzene oxidation during long-term tests within 24 h at 300 °C over Au/Cu-Ce 2:1 and Au/Cu-Ce 1:5 samples. Table S1. Benzene conversion degree depending on temperature over the studied samples. Table S2. Comparison of the activity in benzene oxidation over various samples.

Author Contributions: Conceptualization, T.T.; investigation, P.P., Y.K., G.A. and E.K.; writing—original draft preparation, T.T. and L.I.; writing—review and editing, T.T. and L.I. All authors have read and agreed to the published version of the manuscript.

Funding: This work was supported by the European Regional Development Fund within the Operational Programme "Science and Education for Smart Growth 2014–2020", Project CoE "National center of mechatronics and clean technologies "BG05M2OP001-1.001-0008". The APC was sponsored by MDPI.

Data Availability Statement: The data presented in this study are available in the article.

Conflicts of Interest: The authors declare no conflict of interest.

References

1. Guo, Y.; Wen, M.; Li, G.; An, T. Recent advances in VOC elimination by catalytic oxidation technology onto various nanoparticles catalysts: A critical review. *Appl. Catal. B Environ.* **2021**, *281*, 119447. [CrossRef]
2. Brummer, V.; Teng, S.Y.; Jecha, D.; Skryja, P.; Vavrcikova, V.; Stehlik, P. Contribution to cleaner production from the point of view of VOC emissions abatement: A review. *J. Cleaner Prod.* **2022**, *361*, 132112. [CrossRef]

3. Kamal, M.S.; Razzak, S.A.; Hossain, M.M. Catalytic oxidation of volatile organic compounds (VOCs) A review. *Atmos. Environ.* **2016**, *140*, 117–134. [CrossRef]
4. He, C.; Cheng, J.; Zhang, X.; Douthwaite, M.; Pattisson, S.; Hao, Z. Recent advances in the catalytic oxidation of volatile organic compounds: A review based on pollutant sorts and sources. *Chem. Rev.* **2019**, *119*, 4471–4568. [CrossRef] [PubMed]
5. Gelles, T.; Krishnamurthy, A.; Adebayo, B.; Rownaghi, A.; Rezaei, F. Abatement of gaseous volatile organic compounds: A material perspective. *Catal. Today* **2020**, *350*, 3–18. [CrossRef]
6. Li, J.; Liu, H.; Deng, Y.; Liu, G.; Chen, Y.; Yang, J. Emerging nanostructured materials for the catalytic removal of volatile organic compounds. *Nanotechnol. Rev.* **2016**, *5*, 147–181. [CrossRef]
7. Trovarelli, A. Catalytic properties of ceria and CeO_2-containing materials. *Catal. Rev. Sci. Eng.* **1996**, *38*, 439–520. [CrossRef]
8. Vita, A. Catalytic applications of CeO_2-based materials. *Catalysts* **2020**, *10*, 576. [CrossRef]
9. Montini, T.; Melchionna, M.; Monai, M.; Fornasiero, P. Fundamentals and catalytic applications of CeO_2-based materials. *Chem. Rev.* **2016**, *116*, 5987–6041. [CrossRef]
10. Yang, C.; Lu, Y.; Zhang, L.; Kong, Z.; Yang, T.; Tao, L.; Zou, Y.; Wang, S. Defect engineering on CeO2-based catalysts for heterogeneous catalytic applications. *Small Struct.* **2021**, *2*, 2100058. [CrossRef]
11. Konsolakis, M. The role of copper-ceria interactions in catalysis science: Recent theoretical and experimental advances. *Appl. Catal. B Environ.* **2016**, *198*, 49–66. [CrossRef]
12. Konsolakis, M.; Lykaki, M. Recent advances on the rational design of non-precious metal oxide catalysts exemplified by CuOx/CeO_2 binary system: Implications of size, shape and electronic effects on intrinsic reactivity and metal-support interactions. *Catalysts* **2020**, *10*, 160. [CrossRef]
13. Delimaris, D.; Ioannides, T. VOC oxidation over CuO-CeO_2 catalysts prepared by a combustion method. *Appl. Catal. B Environ.* **2009**, *89*, 295–302. [CrossRef]
14. Piumetti, M.; Bensaid, S.; Andana, T.; Russo, N.; Pirone, R.; Fino, D. Cerium-copper oxides prepared by solution combustion synthesis for total oxidation reactions: From powder catalysts to structured reactors. *Appl. Catal. B Environ.* **2017**, *205*, 455–468. [CrossRef]
15. Hou, J.; Hua, J.; Chang, L.; Wang, J.; Zeng, Z.; Wu, D.; Cui, X.; Bao, W.; Yao, J. Synergistic effects between highly dispersed CuO_x and the surface Cu-[O_x]-Ce structure on the catalysis of benzene combustion. *J. Catal* **2022**, *408*, 9–23. [CrossRef]
16. Saqer, S.M.; Kondarides, D.I.; Verykios, X.E. Catalytic oxidation of toluene over binary mixtures of copper, manganese and cerium oxides supported on γ-Al_2O_3. *Appl. Catal. B Environ.* **2011**, *103*, 275–286. [CrossRef]
17. Menon, U.; Poelman, H.; Bliznuk, V.; Galvita, V.V.; Poelman, D.; Marin, G.B. Nature of the active sites for the total oxidation of toluene by CuO-CeO_2/Al_2O_3. *J. Catal.* **2012**, *295*, 91–103. [CrossRef]
18. Tsoncheva, T.; Issa, G.; Blasco, T.; Dimitrov, M.; Popova, M.; Hernández, S.; Kovacheva, D.; Atanasova, G.; López Nieto, J.M. Catalytic VOCs elimination over copper and cerium oxide modified mesoporous SBA-15 silica. *Appl. Catal. A Gen.* **2013**, *453*, 1–12. [CrossRef]
19. Sumrunronnasak, S.; Chanlek, N.; Pimpha, N. Improved $CeCuO_x$ catalysts for toluene oxidation prepared by aqueous cationic surfactant precipitation method. *Mater. Chem. Phys.* **2018**, *216*, 143–152. [CrossRef]
20. Zeng, Y.; Wang, Y.; Song, F.; Zhang, S.; Zhong, Q. The effect of CuO loading on different method prepared CeO_2 catalyst for toluene oxidation. *Sci. Total Environ.* **2020**, *712*, 135635. [CrossRef]
21. Li, L.; Zhang, C.; Chen, F.; Xiang, Y.; Yan, J.; Chu, W. Facile fabrication of hollow structured Cu-Ce binary oxides and their catalytic properties for toluene combustion. *Catal. Today* **2021**, *376*, 239–246. [CrossRef]
22. Zeng, Y.; Haw, K.G.; Wang, Z.; Wang, Y.; Zhang, S.; Hongmanorom, P.; Zhong, Q.; Kawi, S. Double redox process to synthesize CuO–CeO_2 catalysts with strong Cu-Ce interaction for efficient toluene oxidation. *J. Hazard. Mater.* **2021**, *404*, 124088. [CrossRef] [PubMed]
23. Song, B.; Li, C.; Du, X.; Li, S.; Zhang, Y.; Lyu, Y.; Zhou, Q. Superior performance of Cu-Ce binary oxides for toluene catalytic oxidation: Cu-Ce synergistic effect and reaction pathways. *Fuel* **2021**, *306*, 121654. [CrossRef]
24. Yun, J.; Wu, L.; Hao, Q.; Teng, Z.; Gao, X.; Dou, B.; Bin, F. Non-equilibrium plasma enhanced oxygen vacancies of CuO/CeO_2 nanorod catalysts for toluene oxidation. *J. Environ. Chem. Eng.* **2022**, *10*, 107847. [CrossRef]
25. Zhou, G.; Lan, H.; Gao, T.; Xie, H. Influence of Ce/Cu ratio on the performance of ordered mesoporous CeCu composite oxide catalysts. *Chem. Eng. J.* **2014**, *246*, 53–63. [CrossRef]
26. Kim, S.C. The catalytic oxidation of aromatic hydrocarbons over supported metal oxide. *J. Hazard. Mater.* **2002**, *91*, 285–299. [CrossRef]
27. Hu, C.; Zhu, Q.; Jiang, Z.; Zhang, Y.; Wang, Y. Preparation and formation mechanism of mesoporous CuO-CeO_2 mixed oxides with excellent catalytic performance for removal of VOCs. *Microporous Mesoporous Mater.* **2008**, *113*, 427–434. [CrossRef]
28. Hu, C.; Zhu, Q.; Chen, L.; Wu, R. CuO-CeO_2 binary oxide nanoplates: Synthesis, characterization, and catalytic performance for benzene oxidation. *Mater. Res. Bull.* **2009**, *44*, 2174–2180. [CrossRef]
29. Jung, W.Y.; Lim, K.T.; Hong, S.S. Catalytic combustion of benzene over CuO-CeO_2 mixed oxides. *J. Nanosci. Nanotechnol.* **2014**, *14*, 8507–8511. [CrossRef]
30. Tabakova, T.; Kolentsova, E.; Dimitrov, D.; Ivanov, K.; Manzoli, M.; Venezia, A.M.; Karakirova, Y.; Petrova, P.; Nihtianova, D.; Avdeev, G. CO and VOCs catalytic oxidation over alumina supported Cu-Mn catalysts: Effect of Au or Ag deposition. *Topics Catal.* **2017**, *60*, 110–122. [CrossRef]

31. Haruta, M. Gold as a catalyst in the 21st century: Preparation, working mechanism and applications. *Gold Bull.* **2004**, *37*, 27–36. [CrossRef]
32. Bond, G.C.; Louis, C.; Thompson, D.T. *Catalysis by Gold*; Imperial College Press: London, UK, 2006.
33. Scire, S.; Liotta, L.F. Supported gold catalysts for the total oxidation of volatile organic compounds. *Appl. Catal. B Environ.* **2012**, *125*, 222–246. [CrossRef]
34. Barakat, T.; Rooke, J.C.; Genty, E.; Cousin, R.; Siffert, S.; Su, B.L. Gold catalysts in environmental remediation and water-gas shift technologies. *Energy Environ. Sci.* **2013**, *6*, 371–391. [CrossRef]
35. Centeno, M.A.; Paulis, M.; Montes, M.; Odriozola, J.A. Catalytic combustion of volatile organic compounds on $Au/CeO_2/Al_2O_3$ and Au/Al_2O_3 catalysts. *Appl. Catal. A Gen.* **2002**, *234*, 65–78. [CrossRef]
36. Andreeva, D.; Nedyalkova, R.; Ilieva, L.; Abrashev, M.V. Nanosize gold-ceria catalysts promoted by vanadia for complete benzene oxidation. *Appl. Catal. A Gen.* **2003**, *246*, 29–38. [CrossRef]
37. Lai, S.Y.; Qiu, Y.; Wang, S. Effects of the structure of ceria on the activity of gold/ceria catalysts for the oxidation of carbon monoxide and benzene. *J. Catal.* **2006**, *237*, 303–313. [CrossRef]
38. Ilieva, L.; Petrova, P.; Liotta, L.F.; Sobczak, J.W.; Lisowski, W.; Kaszkur, Z.; Munteanu, G.; Tabakova, T. Gold catalysts on Y-doped ceria supports for complete benzene oxidation. *Catalysts* **2016**, *6*, 99. [CrossRef]
39. Gaálová, J.; Topka, P. Gold and ceria as catalysts for VOC abatement: A review. *Catalysts* **2021**, *11*, 789. [CrossRef]
40. Ivanov, K.; Kolentsova, E.N.; Dimitrov, D.Y. Alumina supported copper-manganese catalysts for combustion of exhaust gases: Effect of preparation method. *Int. J. Chem. Mol. Eng.* **2015**, *9*, 311–320.
41. Kolentsova, E.N.; Dimitrov, D.Y.; Ivanov, K.I.; Tabakova, T.T.; Karakirova, Y.G.; Tenchev, K.K.; Avdeev, G.V. CO and VOCs oxidation over alumina supported Cu-Mn catalysts modified by cerium. *Bulg. Chem. Commun.* **2017**, *49*, 59–66.
42. Bortolotti, M.; Lutterotti, L.; Lonardelli, I. ReX: A computer program for structural analysis using powder diffraction data. *J. Appl. Cryst.* **2009**, *42*, 538–539. [CrossRef]
43. Yu, Y.; Takei, T.; Ohashi, H.; He, H.; Zhang, X.; Haruta, M. Pretreatments of Co_3O_4 at moderate temperature for CO oxidation at −80 °C. *J. Catal.* **2009**, *267*, 121–128. [CrossRef]
44. Wolski, L.; Sobczak, I.; Ziolek, M. Development of multifunctional gold, copper, zinc, niobium containing MCF catalysts—Surface properties and activity in methanol oxidation. *Microporous Mesoporous Mater.* **2017**, *243*, 339–350. [CrossRef]
45. Guzmán, C.; Del Angel, G.; Gómez, R.; Galindo, F.; Zanella, R.; Torres, G.; Angeles-Chavez, C.; Fierro, J.L.G. Gold particle size determination on Au/TiO_2-CeO_2 catalysts by means of carbon monoxide, hydrogen chemisorption and transmission electron microscopy. *J. Nano Res.* **2009**, *5*, 13–23. [CrossRef]
46. Yang, Z.; Wang, Q.; Wei, S. The synergistic effects of the Cu-CeO_2(111) catalysts on the adsorption and dissociation of water molecules. *Phys. Chem. Chem. Phys.* **2011**, *13*, 9363–9373. [CrossRef]
47. Sudarsanam, P.; Hillary, B.; Amin, M.H.; Rockstro, N.; Bentrup, U.; Brückner, A.; Bhargava, S.K. Heterostructured copper–ceria and iron–ceria nanorods: Role of morphology, redox, and acid properties in catalytic diesel soot combustion. *Langmuir* **2018**, *34*, 2663–2673. [CrossRef]
48. Zhu, J.K.; Gao, Q.M.; Chen, Z. Preparation of mesoporous copper cerium bimetal oxides with high performance for catalytic oxidation of carbon monoxide. *Appl. Catal. B Environ.* **2008**, *81*, 236–243. [CrossRef]
49. Shim, J.O.; Na, H.S.; Jha, A.; Jang, W.J.; Jeong, D.W.; Nah, I.W.; Jeon, B.H.; Rohp, H.S. Effect of preparation method on the oxygen vacancy concentration of CeO_2-promoted Cu/Al_2O_3 catalysts for HTS reactions. *Chem. Eng. J.* **2016**, *306*, 908–915. [CrossRef]
50. Ilieva, L.; Ivanov, I.; Petrova, P.; Munteanu, G.; Karakirova, Y.; Sobczak, J.W.; Lisowski, W.; Anghel, E.M.; Kaszkur, Z.; Tabakova, T. Effect of Y-doping on the catalytic properties of CuO/CeO_2 catalysts for water-gas shift reaction. *Int. J. Hydrog. Energy* **2020**, *45*, 26286–26299. [CrossRef]
51. Ratnasamy, P.; Srinivas, D.; Satyanarayana, C.V.V.; Manikandan, P.; Kumaran, R.S.S.; Sachin, M.; Shetti, V.N. Influence of the support on the preferential oxidation of CO in hydrogen-rich steam reformates over the CuO–CeO_2–ZrO_2 system. *J. Catal.* **2004**, *221*, 455–465. [CrossRef]
52. Yao, H.C.; Yao, Y.F.Y. Ceria in automotive exhaust catalysts: I. Oxygen storage. *J. Catal.* **1984**, *86*, 254–265. [CrossRef]
53. Laachir, A.; Perrichon, V.; Bardi, A.; Lamotte, J.; Catherine, E.; Lavalley, J.C.; El Fallah, J.; Hilaire, L.; Le Normand, F.; Quemere, E.; et al. Reduction of CeO_2 by hydrogen. *J. Chem. Soc. Faraday. Trans.* **1991**, *7*, 1601–1609. [CrossRef]
54. Avgouropoulos, G.; Ioannides, T. Effect of synthesis parameters on catalytic properties of CuO-CeO_2. *Appl. Catal. B Environ.* **2006**, *67*, 1–11. [CrossRef]
55. Mrabet, D.; Abassi, A.; Cherizol, R.; Do, T.-O. One-pot solvothermal synthesis of mixed Cu-Ce-O_x nanocatalysts and their catalytic activity for low temperature CO oxidation. *Appl. Catal. A Gen* **2012**, *447–448*, 60–66. [CrossRef]
56. Sun, S.; Mao, D.; Yu, J. Enhanced CO oxidation activity of CuO/CeO_2 catalyst prepared by surfactant-assisted impregnation method. *J. Rare Earths* **2015**, *33*, 1268–1274. [CrossRef]
57. Li, Y.; Fu, Q.; Flytzani-Stephanopoulos, M. Low-temperature water-gas shift reaction over Cu- and Ni-loaded cerium oxide catalysts. *Appl. Catal. B Environ.* **2000**, *27*, 179–191. [CrossRef]
58. Lykaki, M.; Pachatouridou, E.; Carabineiro, S.A.C.; Iliopoulou, E.; Andriopoulou, C.; Kallithrakas-Kontos, N.; Boghosian, S.; Konsolakis, M. Ceria nanoparticles shape effects on the structural defects and surface, chemistry: Implications in CO oxidation by Cu/CeO_2 catalysts. *Appl. Catal. B Environ.* **2018**, *230*, 18–28. [CrossRef]

59. Zeng, S.; Bai, X.; Wang, X.; Yu, W.; Liu, Y. Valence state of active copper in CuO_x/CeO_2 catalysts for CO oxidation. *J. Rare Earths* **2006**, *24*, 177–181. [CrossRef]
60. Martınez-Arias, A.; Fernandez-Garcıa, M.; Soria, J.; Conesa, J.C. Spectroscopic study of a Cu/CeO_2 catalyst subjected to redox treatments in carbon monoxide and oxygen. *J. Catal.* **1999**, *182*, 367–377. [CrossRef]
61. Liu, Y.; Mao, D.; Yu, J.; Zheng, Y.; Guo, X. Facile preparation of highly active and stable $CuO\text{-}CeO_2$ catalysts for low-temperature CO oxidation via direct solvothermal method. *Catal. Sci. Technol.* **2020**, *10*, 8385–8395. [CrossRef]
62. Andreeva, D.; Idakiev, V.; Tabakova, T.; Ilieva, L.; Falaras, P.; Bourlinos, A.; Travlos, A. Low-temperature water-gas shift reaction over Au/CeO_2 catalysts. *Catal. Today* **2002**, *72*, 51–57. [CrossRef]
63. Tabakova, T.; Ilieva, L.; Petrova, P.; Venezia, A.M.; Avdeev, G.; Zanella, R.; Karakirova, Y. Complete benzene oxidation over mono and bimetallic Au-Pd catalysts supported on Fe-modified ceria. *Chem. Eng. J.* **2015**, *260*, 133–141. [CrossRef]
64. Wang, A.; Liu, X.Y.; Mou, C.Y.; Zhang, T. Understanding the synergistic effects of gold bimetallic catalysts. *J. Catal.* **2013**, *308*, 258–271. [CrossRef]
65. Grzelak, K.; Sobczak, I.; Yang, C.-M.; Ziolek, M. Gold-copper catalysts supported on SBA-15 with long and short channels—Characterization and the use in propene oxidation. *Catal. Today* **2020**, *356*, 155–164. [CrossRef]
66. Galvita, V.V.; Filez, M.; Poelman, H.; Bliznuk, V.; Marin, G.B. The role of different types of CuO in $CuO\text{-}CeO_2/Al_2O_3$ for total oxidation. *Catal. Lett.* **2014**, *144*, 32–43. [CrossRef]
67. Deshpande, S.; Patil, S.; Kuchibhatla, S.V.; Seal, S. Size dependency variation in lattice parameter and valency states in nanocrystalline cerium oxide. *Appl. Phys. Lett.* **2005**, *87*, 133113.